

A Wireless AI-Generated Content (AIGC) Provisioning Framework Empowered by Semantic Communication

Runze Cheng, *Student Member, IEEE*, Yao Sun, *Senior Member, IEEE*, Dusit Niyato, *Fellow, IEEE*, Lan Zhang, *Senior Member, IEEE*, Lei Zhang, *Senior Member, IEEE*, and Muhammad Imran, *Fellow, IEEE*

Abstract—Generative AI applications are recently catering to a vast user base by creating diverse and high-quality AI-generated content (AIGC). With the proliferation of mobile devices and rapid growth of mobile traffic, providing ubiquitous access to high-quality AIGC services via wireless communication networks is becoming the future direction for AIGC products. However, it is challenging to provide optimal AIGC services in wireless networks with unstable channels, limited bandwidth resources, and unevenly distributed computational resources. To tackle these challenges, we propose a semantic communication (SemCom)-empowered AIGC (SemAIGC) generation and transmission framework, where only semantic information of the content rather than all the binary bits should be extracted and transmitted by using SemCom. Specifically, SemAIGC integrates diffusion-based models within the semantic encoder and decoder for efficient content generation and flexible adjustment of the computing workload of both transmitter and receiver. Meanwhile, we devise a resource-aware workload trade-off (ROOT) scheme into the SemAIGC framework to intelligently decide transmitter/receiver workload, thus adjusting the utilization of computational resource according to service requirements. Simulations verify the superiority of our proposed SemAIGC framework in terms of latency and content quality compared to conventional approaches.

Index Terms—AI-generated content, Semantic communication, Diffusion model, Intelligent workload allocation

I. INTRODUCTION

Driven by recent advancements in deep learning and computing devices, generative AI has demonstrated remarkable strides in analyzing various forms of media and creating AI-generated content (AIGC) [1]. For the delivery of high-quality content, well-crafted AIGC models have evolved to maintain millions of parameters within their neural networks, a feat that can necessitate a large-scale server devour thousands of hours of graphics processing unit (GPU) time in a single model training session [2]. Limited by the computing-intensive nature of AIGC, existing AIGC applications, including notable products like ChatGPT, DELL-R-2, and ERNIE Bot, predominantly find their home on cloud servers equipped with ample computational resources [3].

Runze Cheng, Yao Sun, Lei Zhang, and Muhammad Ali Imran are with the James Watt School of Engineering, University of Glasgow, Glasgow G12 8QQ, U.K.

Dusit Niyato is with the School of Computer Science and Engineering, Nanyang Technological University, 639798, Singapore.

Lan Zhang is with the Department of Electrical and Computer Engineering, Michigan Technological University, Houghton, MI 49931 USA.

Yao Sun is the corresponding author. (Email: Yao.Sun@glasgow.ac.uk)

A. Background: AIGC in Wireless

Due to the rapid development of mobile technology and the increasing adoption of smartphones, tablets, IoT devices, and other mobile gadgets, the percentage of global Internet traffic on mobile devices has surged over the past decade. In 2022, it was estimated that there were over 15 billion mobile devices worldwide, which contributed 55% of global Internet traffic [4]. In this background, many AI companies are actively strategizing and positioning themselves in the realm of mobile device-oriented AIGC applications. Nevertheless, wireless AIGC services demand both satisfied content quality and latency, which are challenging to ensure under dynamic wireless channels. Moreover, these services often grapple with limited communication resources (like bandwidth, and high-quality channels) and unevenly distributed computational resources (such as computing power) in wireless networks. Therefore, more efficient and accessible AIGC generation and transmission frameworks are required in wireless AIGC networks.

Recently, a few studies about wireless AIGC generation and transmission have been conducted to improve the utilization of unevenly distributed computational resources. The authors in [5] proposed a wireless AIGC network architecture where cloud servers primarily handle computationally intensive AIGC model pre-training. Additionally, it offloads content generation tasks from cloud servers to edge transmitters. In [6], a dynamic AIGC service provider selection scheme is proposed in an intelligent wireless AIGC network to enable users to connect to the provider that owns suitable edge servers and enough computational resources. Considering the limited bandwidth resources and dynamic channel quality of wireless networks, the authors in [7] developed a pricing-based incentive mechanism for AIGC generation and transmission framework to maximize users' utility in mobile edge networks. Among these existing works, a common bottleneck is that the available communication resources in wireless networks are insufficient to cope with the potentially overwhelming number of service requests that users may raise to edge transmitters in the near future.

In parallel, some research works aim to overcome the limitation of communication resources in the wireless network. As lightweight AIGC models have been tested and certified in some works [8], [9], it is becoming capable of deploying AIGC models on local mobile devices with limited computational

resources. Under this premise, a novel collaborative distributed AIGC framework is conceptualized in [10], which allows smartphones to process the diffusion model locally in an edge server-empowered wireless AIGC network. However, considering the computational resource limitation of mobile devices, the generated content quality and content-generating latency are difficult to ensure.

B. Motivation

To provide suitable AIGC services in wireless networks, it is imperative to explore a wireless AIGC service provisioning framework that can meet diverse service requirements under limited communication resources, unevenly distributed computational resources, and dynamic channel quality.

Semantic communications (SC), as the breakthrough beyond the Shannon paradigm, aims to effectively transmit necessary semantic information of source signal, as opposed to the accurate reception of every single binary bit of source signal without considering its meaning [11]. In SemCom, the encoder is utilized to extract necessary semantic information, and then fewer bandwidth resources are consumed in transmitting compressed information [12]. Meanwhile, the receiver accurately interprets semantic information from transmitted bits and reduces semantic distortion caused by channel noise, thus improving transmission reliability at a semantic level [13]. Thanks to these superiorities, SemCom is validated to be powerful in the end-to-end transmission for delivering of high-quality content. In [14], the authors designed a group of joint source-channel coding algorithms to encode and decode images over multiple channels, allowing flexible and adaptive bandwidth transmissions. In parallel, a high-efficiency deep joint source-channel encoding method is proposed in [15] to adaptively extract semantic features across video frames under different channel conditions.

With these superiorities, combining SemCom with generative AI models is promising to provide AIGC service over wireless networks with limited communication resources and unevenly distributed computational resources. Since the generated semantic information is transmitted instead of the entire bits of content, the pressure of communication resources can be reduced with a slim data size. Additionally, the received semantic information can be decoded into high-quality content by identifying meaningful semantic information while removing noise, thus allowing for suitable AIGC services in a harsh channel quality.

However, resources in wireless networks, such as bandwidth, GPU/CPU cores, and computational power, are often with dynamic availability. Therefore, it is inefficient to directly integrate SemCom and generative AI, where the structure of encoders and decoders is fixed. This fixed structure makes the encoder/decoder unable to adjust the computing workloads according to the resource availability. Furthermore, in the fixed structure of the encoder and decoder, the semantic density is unadjustable, causing the semantic noise ratio to rise with increasing noise density, thus posing additional denoising difficulty during decoding. Meanwhile, considering the changing preferences of users when accessing AIGC service, they may

have varying service requirements, such as latency and content quality. Since the semantic computing workloads and semantic density are unadjustable in the transceiver, meeting these requirements becomes a difficulty.

In response to the unsolved difficulties, employing diffusion-based models and machine learning (ML) in the joint AIGC generation and transmission is a potential solution. The diffusion-based semantic processing models are utilized to denoising irrelevant information from pure Gaussian noise and finally retain valid information of content like text [16], audio [17], or image [18]. By deploying diffusion models into the encoder and decoder, it is promising to develop a workload-adjustable transceiver, in which the computing workloads and resources utilization can be altered with the denoising steps. Simultaneously, harnessing the capabilities of powerful neural networks, ML is capable of intelligently deciding the denoising steps of the encoder and decoder, i.e., making workload trade-off, thus meeting the computing latency requirement [19]. Furthermore, the semantic density can be also optimized to reduce the semantic noise ratio, thus efficiently ensuring that the content quality is consistent and satisfies the requirements under varying channel qualities.

C. Contributions and Organization

In this paper, to narrow down our focus, we delve specifically into image-based service provisioning in wireless networks. We first propose a SemCom-empowered AIGC (SemAIGC) framework to jointly generate and transmit images in wireless networks. In SemAIGC, we deploy the diffusion models within the AIGC encoder-decoder to establish a workload-adjustable transceiver. In addition, a deep reinforcement learning (DRL)-based resource-aware workload trade-off (ROOT) scheme is developed in the SemAIGC framework to intelligently adjust resource usage and service quality. Simulation results demonstrate the effectiveness and robustness of our proposed SemAIGC under dynamic resource availability, varying channel quality, and diverse service requirements. The main contributions of the paper are summarized as follows:

- We propose a wireless SemAIGC framework to provide appropriate AIGC access service under constrained communication resources and unevenly distributed computational resources.
- We design a workload-adjustable AIGC transceiver in the SemAIGC framework, which deploys the diffusion-based encoder and decoder to allow for flexible allocation of the computing workload at both the transmitter and receiver.
- In order to support diverse AIGC service requirements from users under dynamic resource availability and channel quality, we formulate the problem of AIGC workload allocation as a Markov decision process (MDP) problem and propose the ROOT scheme to intelligently make the workload trade-off decisions.

This paper is organized as follows. In Section II, we present the detailed SemAIGC framework, followed by the design of edge transmitter and local receiver in Section III. The problem formulation and ROOT scheme design are elaborated in Section IV. Then, we evaluate the performance gain of the

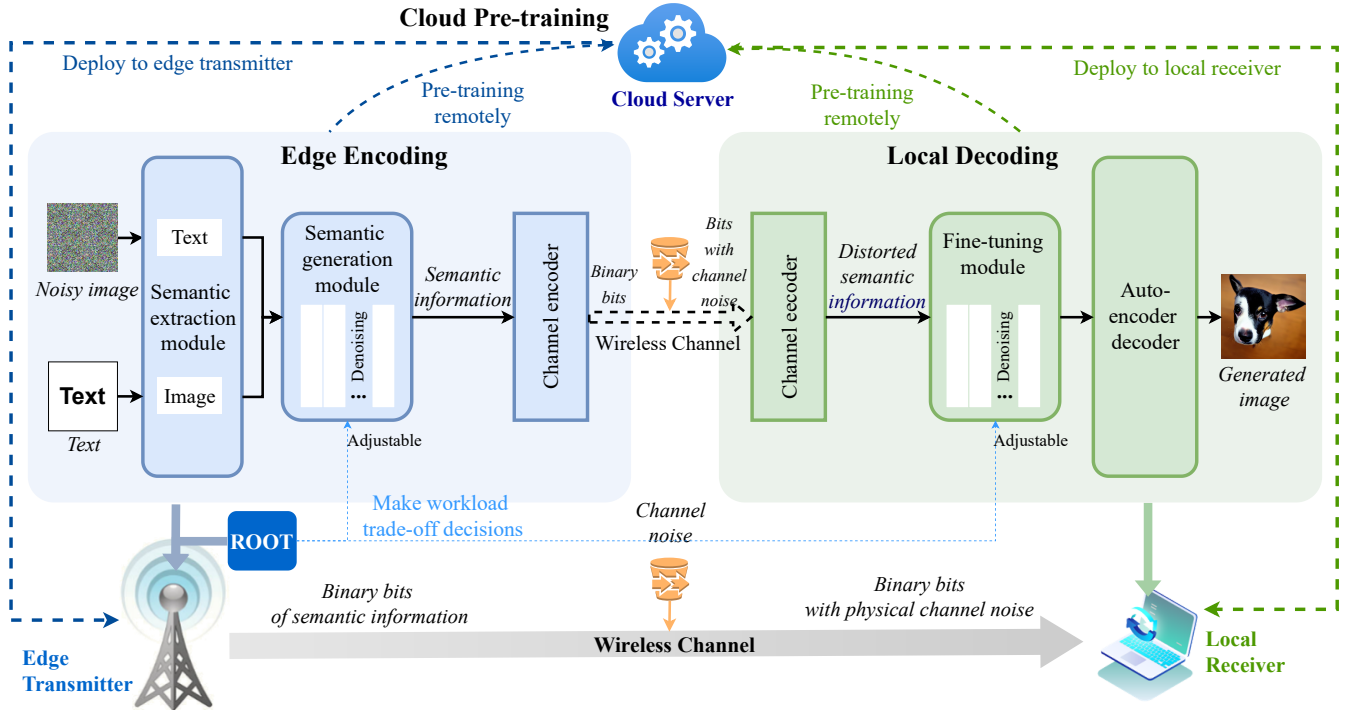


Fig. 1. The proposed SemaAIGC framework.

SemaAIGC framework and ROOT scheme by simulations in Section V. Section VI concludes the paper.

II. SEMCOM-EMPOWERED AIGC GENERATION AND TRANSMISSION FRAMEWORK

Given the unevenly distributed computational resources and limited communication resources, we introduce the SemaAIGC framework, as shown in Fig. 1. In this framework, our specific focus revolves around the generation of images from textual descriptions, namely text-to-image (T2I). The image generation and transmission in this framework can be categorized into three main stages, i.e., cloud pre-training, edge encoding, and local decoding.

A. Cloud Pre-training

In SemaAIGC, we utilize a cloud server to conduct the T2I model training processes. Generally, a high-quality T2I model requires millions of parameters in a total size of 1-10 GB, stringent requirements are exposed for specialized hardware like GPU, CPU, and capable devices during its training. Cloud servers as a centralized infrastructure with ample computing power, storage, database, etc. are well matched to the demands. As shown in Fig. 1, the cloud server retains the copy of all the modules within both the encoder and decoder. After feeding these modules with a substantial corpus of text-image pairs, the edge transmitter and local receiver can download the pre-trained encoder and decoder from the cloud server, respectively. Additionally, the encoder and decoder can be periodically updated within the cloud server, while the edge transmitter and local receiver do not require further training before using them to offer AIGC access services. Moreover, the

neural network of the ROOT scheme is also trained remotely and later deployed in the edge transmitter and fine-tuned according to the local wireless communication environment.

B. Edge Encoding

As shown in Fig. 1, the edge transmitter is composed of a semantic extraction module, a semantic generation module, and a channel encoder. The semantic extraction module comprises two independent networks, responsible for extracting semantic information from text and images, respectively. As the core of the edge transmitter, the semantic generation module uses a diffusion model to predict and gradually denoise data starting from pure noise according to the provided textual description. Compared with the pre-training stage, lower computational resources are required in the AIGC generation and transmission stage. Therefore, the transmitter with edge computing servers is sufficient to run these modules with acceptable computing latency. Apart from the semantic encoder, the channel encoder in Fig. 1 is deployed at the edge transmitter to convert semantic information into binary bit signals.

C. Local Decoding

With the improvement of computing power in mobile devices, plenty of user devices are capable of executing the relatively simple information fine-tuning and recovery process. In the proposed SemaAIGC framework, the T2I decoder of a local receiver in Fig. 1 is composed of a semantic fine-tuning module, an autoencoder decoder module, and a channel decoder. Specifically, the channel decoder transfers the binary bits into semantic information and detects the noise distribution of delivered information. Given the computing power

for local devices, a lightweight diffusion model is deployed into the semantic fine-tuning module. After a rapid fine-tuning process, the semantic noise can be eliminated, and then the autoencoder decoder module transfers semantic information into high-resolution images with text guidance.

III. WORKLOAD-ADJUSTABLE TRANSCEIVER DESIGN

In this section, we consider a downlink transmission scenario, where the image semantic information is generated at the edge transmitter and then transmitted to the local receiver for further fine-tuning via a wireless channel. The edge transmitter and local receiver design of the SemAIGC framework are detailed in the following.

A. Encoder Design at Edge Transmitter

We first present the semantic extraction module, semantic generation module, and channel encoder deployed in the edge transmitter, as shown in the upper half of Fig 2.

1) *Semantic extraction module*: Let s_{text} and s denote the input text signal and image signal of the semantic extraction module, respectively. The semantic information extracted from the text signal and that from the image signal are represented as z_{text} and z , respectively. As the guidance of image generation, the semantic information of text z_{text} is extracted by a contrastive language-image pre-training (CLIP) encoder [20] as a sequence. Meanwhile, by using an attention-based variational autoencoder (VAE) model [21], the input image is encoded into Gaussian-like distribution and outputs multiple sets of means and standard deviations. Then, we use these values to generate latent space image z , i.e., image semantic information. Note that the semantic information of real image is only used during the model training stage and is not directly involved in the T2I generation. The two modalities' semantic information is extracted as follows:

$$z_{text} = \mathcal{E}(s_{text}; \varphi_{text}), z = \mathcal{E}(s; \varphi). \quad (1)$$

Here, $\mathcal{E}(\cdot; \varphi_{text})$ and $\mathcal{E}(\cdot; \varphi)$ are the text encoder and image encoder with learnable parameters φ_{text} and φ , respectively.

2) *Semantic-generating module*: The semantic generation modules in Fig. 2 is based on the denoising diffusion probabilistic models (DDPMs), consisting of two processes: the diffusion process and the reverse diffusion process [22].

As shown in Fig. 3, the diffusion process is a fixed (or predefined) forward diffusion process, which is denoted as $q(z_t|z_{t-1})$. In the diffusion process, a scheduler gradually adds Gaussian noise at each time step $t \in [0, T]$, until the initial semantic information of an image z_0 becomes pure noise z_T . Basically, each new image at time step t is drawn from a conditional Gaussian distribution as

$$z_t = \sqrt{1 - \beta_t} z_{t-1} + \sqrt{\beta_t} \epsilon, \quad (2)$$

where $0 < \beta_1 < \beta_2 < \dots < \beta_T < 1$ is a known variance schedule with time-related constants, and $\epsilon \sim \mathcal{N}(0, I)$ is the added Gaussian noise with an identity matrix I .

Meanwhile, the reverse diffusion process in Fig. 3 is a denoising process which is represented as $p(z_{t-1}|z_t)$. In this process, a neural network, i.e., UNet [23], is trained to learn

the conditional probability distribution $p_\theta(z_{t-1}|z_t, z_{text})$ and gradually denoise the semantic information according to text semantic starting from pure noise until it ends up with the semantic information of an actual image. Here, θ is the learnable parameters of the UNet, text guidance is implemented by concatenating the text embedding to the key-value pairs of each self-attention layer in the UNet [18]. Accordingly, the reverse diffusion process is

$$z_{t-1} = \frac{1}{\sqrt{\alpha_t}} \left(z_t - \frac{1 - \alpha_t}{\sqrt{1 - \alpha_t}} \epsilon_\theta(z_t, t, z_{text}) \right) + \bar{\sigma}_t \tilde{\epsilon}, \quad (3)$$

where ϵ_θ is the UNet predicted noise, $\alpha_t = 1 - \beta_t, t \in \{1, \dots, T\}$ is a known constant of step t , $\bar{\alpha}_t = \prod_{i=1}^t \alpha_i$ is a cumulative product of α_t , $\bar{\sigma}_t$ is also a time dependent constant of step t , and $\tilde{\epsilon} \sim \mathcal{N}(0, I)$ is the random normal Gaussian noise.

The semantic generation module conducts different processes during the pre-training stage and content-generating stage, i.e., edge encoding stage, as shown in Fig. 3. At the pre-training stage, the semantic generation module executes both two processes to learn the noise distribution, while only involves the reverse diffusion process in content-generating stage. We introduce the content-generating stage here, whereas the model training is elaborated on later in Section IV. C. In the content-generating stage, with pre-trained UNet, the target image is denoised from randomly generated pure noisy data z_T . After the scheduled denoising steps T , the image semantic information is output according to text guidance, which is denoted as

$$z_\theta = \mathcal{F}_1(z_T, T, z_{text}; \theta), \quad (4)$$

where $\mathcal{F}_1(\cdot; \theta)$ is the UNet with learnable parameter θ .

3) *Channel encoder module*: As transmitting image semantic information consumes significantly more communication resources than that of text semantic information, this paper specifically concentrates on image semantic information transmission, while assuming that text semantic information can be received correctly [24]. The channel encoder in this work is deployed to convert image semantic information into binary bit signals. The transmitted signal is encoded as $y = \mathcal{C}(z_\theta)$ by the channel encoder.

We consider the additive white Gaussian noise channel in this paper. When the transmitted signal passes the physical channel, the received signal is expressed as

$$y' = hy + n, \quad (5)$$

where h represents the channel and n is the physical channel noise.

B. Decoder Design at Local Receiver

Then, we present the T2I decoder of the local receiver, which is composed of the channel decoder module, fine-tuning module, and autoencoder decoder module, as shown in the lower half of Fig. 2.

1) *Channel decoder module*: The received binary bit signals are recovered as semantic information by the channel decoder. The decoded signal can be represented as

$$\begin{aligned} z' &= \mathcal{C}^{-1}(y'), \\ z' &\approx z + \epsilon^c, \end{aligned} \quad (6)$$

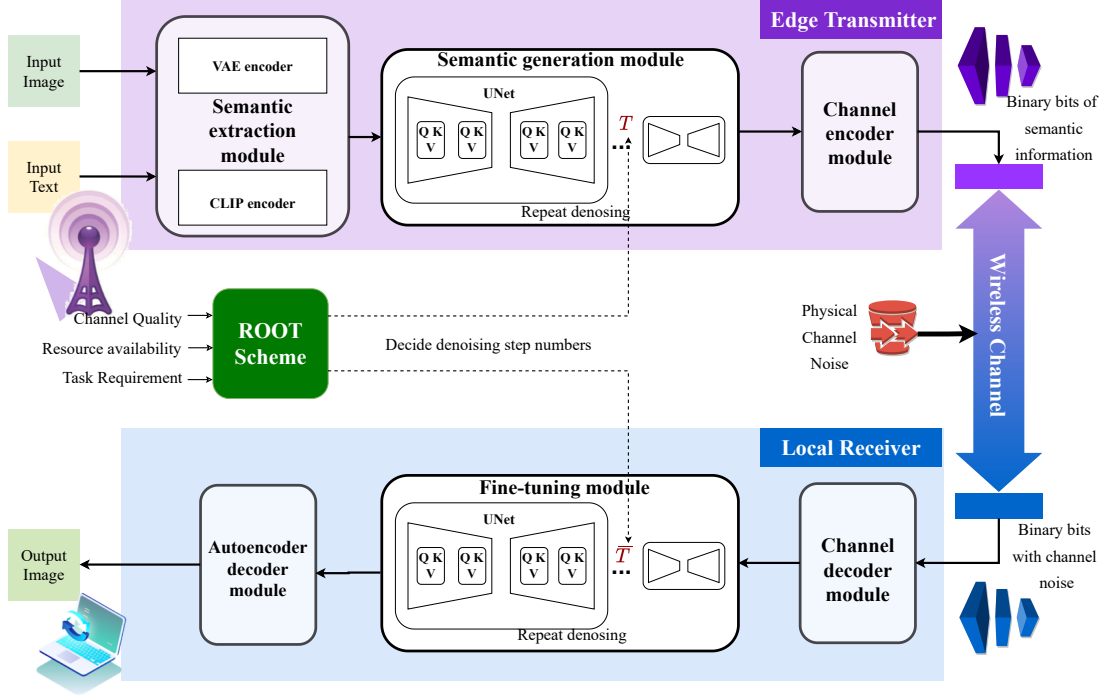


Fig. 2. The workload-adjustable transceiver in SemAIGC.

where \mathcal{C}^{-1} is the channel decoder, and $\epsilon^c \sim \mathcal{N}(0, \sigma^2 I)$ is the *semantic noise* with a variance matrix $\sigma^2 I$ caused by the physical channel noise n .

2) *Fine-tuning module*: This is a lightweight version of the semantic generation module, which is used for fine-tuning decoded image semantic information [25]. The reverse diffusion process of fine-tuning module is as follows

$$z_{\bar{\theta}} = \mathcal{F}_2(z', \bar{T}, z_{text}; \bar{\theta}), \quad (7)$$

where $\mathcal{F}_2(\cdot; \bar{\theta})$ is the UNet with learnable parameter $\bar{\theta}$, \bar{T} is the number of reverse diffusion steps for the fine-tuning module. Nevertheless, unlike the semantic generation module, the fine-tuning module considers semantic noise ϵ^c when training the UNet. The modified diffusion process simulates gradually adding semantic noise ϵ^c to semantic information, and then the reverse diffusion process is capable of removing the semantic noise ϵ^c from semantic information, as proven in the Proposition. 1.

Proposition 1. *Given the semantic noise $\epsilon^c \sim \mathcal{N}(0, \sigma^2 I)$, the first step of reverse diffusion process in the fine-tuning module is as follows:*

$$z_{t-1} = \frac{1}{\sqrt{\alpha_t}} (z_t - C(\alpha, \sigma, t) \epsilon_{\theta}(z_t, t, z_{text})) + \bar{\sigma}_t \epsilon, \quad (8)$$

$$C(\alpha, \sigma, t) = \frac{(1 - \alpha_t + \sigma_{t,t-1}^2) (\sqrt{1 - \hat{\alpha}_t} - \sigma_t^2)}{1 - \hat{\alpha}_t + \sigma_{t-1}^2 \alpha_t + \sigma_{t,t-1}^2},$$

where $\epsilon_{\theta}(z_t, t, z_{text})$ is the noise predicted from semantic information z_t , $C(\alpha, \sigma, t)$ is a time related constant, and $\bar{\sigma}_t$ is a time-dependent constant for the random sample of Gaussian noise.

Proof: When the delivered semantic information is impacted by channel noise, according to (2), the semantic information is

$$\begin{aligned} z_t &= \sqrt{\alpha_t} z_{t-1} + \sqrt{1 - \alpha_t} \epsilon + \epsilon^c \\ &= \sqrt{\alpha_t} z_0 + \sqrt{1 - \hat{\alpha}_t} \epsilon + \epsilon^c, \quad (9) \\ \epsilon^c &\sim \mathcal{N}(0, \sigma^2 I), \epsilon \sim \mathcal{N}(0, I). \end{aligned}$$

However, for model training, we consider that the semantic noise ϵ^c is gradually added in the diffusion steps $\{1, \dots, t, \dots, \bar{T}\}$, then the diffusion process can be formulated as

$$\begin{aligned} z_t &= \sqrt{\alpha_t} (z_{t-1} + \frac{1}{\bar{T} \prod_{j=t}^{\bar{T}} \sqrt{\alpha_j}} \epsilon^c) + \sqrt{1 - \alpha_t} \epsilon \\ &= \sqrt{\hat{\alpha}_t} z_{t-1} + \sqrt{1 - \hat{\alpha}_t} \epsilon + \frac{\sigma}{\bar{T} \prod_{j=t+1}^{\bar{T}} \sqrt{\alpha_j}} \epsilon. \quad (10) \end{aligned}$$

The aim of fine-tuning module is to generate image semantic information z_0 from received semantic information z_t via the reverse diffusion process. Therefore, it is important to predict the distribution probability of the semantic information in the previous step z_{t-1} with the present information z_t , i.e., $q(z_{t-1} | z_t, z_0)$. According to the Bayes' theorem, we have

$$\begin{aligned} q(z_{t-1} | z_t, z_0) &= q(z_t | z_{t-1}, z_0) \frac{q(z_{t-1} | z_0)}{q(z_t | z_0)}, \\ q(z_t | z_0) &\sim \mathcal{N}(\sqrt{\hat{\alpha}_t} z_0, 1 - \hat{\alpha}_t + \sigma_t^2), \\ q(z_{t-1} | z_0) &\sim \mathcal{N}(\sqrt{\hat{\alpha}_{t-1}} z_0, 1 - \hat{\alpha}_{t-1} + \sigma_{t-1}^2), \\ q(z_t | z_{t-1}, z_0) &\sim \mathcal{N}(\sqrt{\hat{\alpha}_t} z_{t-1}, 1 - \alpha_t + \sigma_{t,t-1}^2). \quad (11) \end{aligned}$$

Here, σ_t^2 , σ_{t-1}^2 , and $\sigma_{t,t-1}^2$ are the different noise variances. Then, with the Gaussian distribution formula $f(x) =$

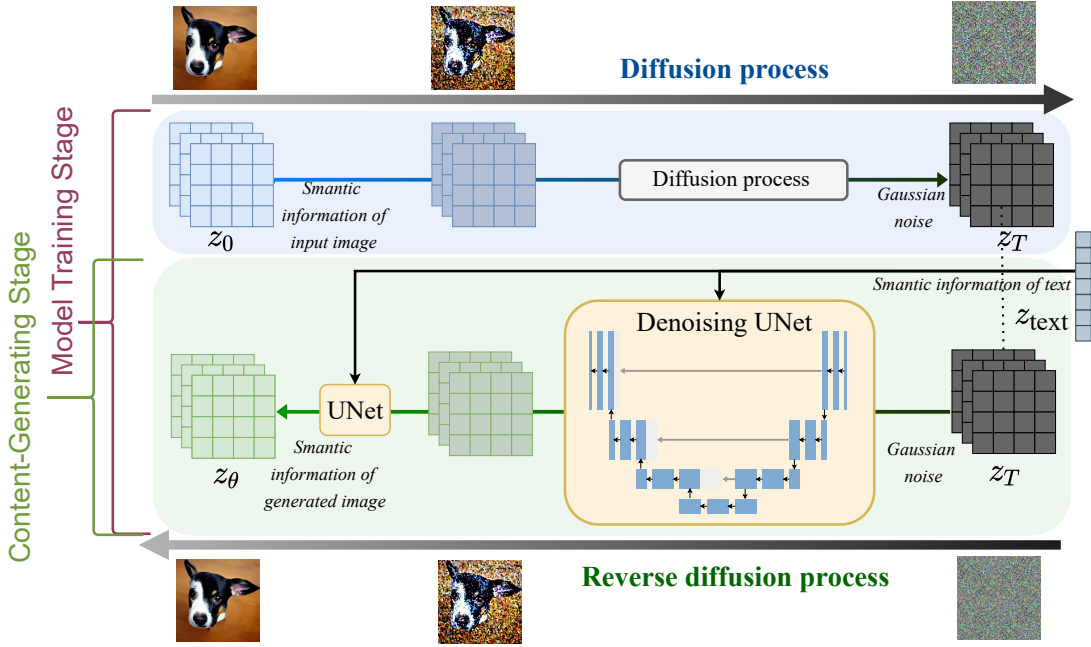


Fig. 3. The diffusion and reverse diffusion processes in the semantic generation module.

$\frac{1}{\sigma\sqrt{2\pi}} \exp\left(-\frac{1}{2}\left(\frac{x-\mu}{\sigma}\right)^2\right)$, we have

$$q(z_{t-1}|z_t, z_0) \propto \frac{1}{\sigma\sqrt{2\pi}} \exp\left(-\frac{1}{2}\left(\frac{(z_t - \sqrt{\dot{\alpha}_t} z_{t-1})^2}{1 - \dot{\alpha}_t + \sigma_{t,t-1}^2} + \frac{(z_{t-1} - \sqrt{\dot{\alpha}_{t-1}} z_0)^2}{1 - \dot{\alpha}_{t-1} + \sigma_{t-1}^2} - \frac{(z_t - \sqrt{\dot{\alpha}_t} z_0)^2}{1 - \dot{\alpha}_t + \sigma_t^2}\right)\right). \quad (12)$$

Since the purpose of the reverse diffusion process is to predict the semantic information in the previous step, while z_t and z_0 are known semantic information, we have

$$q(z_{t-1}|z_t, z_0) \propto \frac{1}{\sigma\sqrt{2\pi}} \times \exp\left(-\frac{1}{2}\left(\left(\frac{\alpha_t}{1 - \dot{\alpha}_t + \sigma_{t,t-1}^2} + \frac{1}{1 - \dot{\alpha}_{t-1} + \sigma_{t-1}^2}\right) z_{t-1}^2 - 2\left(\frac{\sqrt{\dot{\alpha}_t} z_t}{1 - \dot{\alpha}_t + \sigma_{t,t-1}^2} + \frac{\sqrt{\dot{\alpha}_{t-1}} z_0}{1 - \dot{\alpha}_{t-1} + \sigma_{t-1}^2}\right) z_{t-1} + C(z_t, z_0)\right)\right). \quad (13)$$

As Gaussian distribution formula can be transformed as $f(x) = \frac{1}{\sigma\sqrt{2\pi}} \exp\left(-\frac{1}{2}\left(\frac{1}{\sigma^2} x^2 - \frac{2\mu}{\sigma^2} x + \frac{\mu^2}{\sigma^2}\right)\right)$, we can calculate the mean of the distribution as

$$\mu_\theta(z_t, z_0) = \frac{\sqrt{\dot{\alpha}_t} (1 - \dot{\alpha}_{t-1} + \sigma_{t,t-1}^2)}{1 - \dot{\alpha}_t + \sigma_{t,t-1}^2 \alpha_t + \sigma_{t,t-1}^2} z_t + \frac{\sqrt{\dot{\alpha}_{t-1}} (1 - \dot{\alpha}_t + \sigma_{t,t-1}^2)}{1 - \dot{\alpha}_t + \sigma_{t,t-1}^2 \alpha_t + \sigma_{t,t-1}^2} z_0. \quad (14)$$

Then, (10) can be reversed as $z_0 = \frac{1}{\sqrt{\dot{\alpha}_t}} (z_t - (\sqrt{1 - \dot{\alpha}_t} - \sigma_t^2) \epsilon_t)$, $\epsilon_t \sim \mathcal{N}(0, I)$, thus we

have

$$\mu_\theta(z_t, t) = \frac{1}{\sqrt{\dot{\alpha}_t}} \left(z_t - \frac{(1 - \dot{\alpha}_t + \sigma_{t,t-1}^2) (\sqrt{1 - \dot{\alpha}_t} - \sigma_t^2)}{1 - \dot{\alpha}_t + \sigma_{t,t-1}^2 \alpha_t + \sigma_{t,t-1}^2} \epsilon_t \right). \quad (15)$$

Therefore, to sample $z_{t-1} \sim p_{\bar{\theta}}(z_{t-1}|z_t)$ is to compute $z_{t-1} = \frac{1}{\sqrt{\dot{\alpha}_t}} (z_t - C(\alpha, \sigma, t) \epsilon_\theta(x_t, t)) + \bar{\sigma}_t \epsilon$, we prove Proposition 1. ■

3) *Autoencoder decoder module*: This is the decoder of the VAE model with KL loss [26], which paints the final image output using the fused semantic information of text and image. The resolution of the image semantic information increases in this process, till it ultimately becomes the target image. The final image from the autoencoder decoder module is output as

$$\bar{s} = \mathcal{D}(z_{\bar{\theta}}|z_{text}; \bar{\varphi}), \quad (16)$$

where $\mathcal{D}(\cdot; \bar{\varphi})$ is the autoencoder decoder with learnable parameter $\bar{\varphi}$.

C. Training Algorithm

Since we aim to generate a high-quality image from text, the training of image process modules is the major part that we focus, whereas the text-extracting module can use a pre-trained CLIP model. Before presenting the core of T2I generation, i.e., the semantic generation module and the fine-tuning module, we introduce the training of the image semantic extraction module and the autoencoder decoder module. These two modules are jointly trained according to the loss function of the VAE encoder-decoder [26]. In the consideration

of semantic similarity and reconstruction likelihood, the loss function is

$$\begin{aligned} loss_1(\varphi, \bar{\varphi}) &= -\frac{1}{2m} \sum_{i=1}^M \sum_{j=1}^K (1 + \log(\sigma_j^2) - \sigma_j^2 - \mu_j^2) \\ &\quad + \frac{1}{m} \sum_{i=1}^M (s_i - \bar{s}_i)^2 \\ &= -D_{KL}(\tilde{q}_\varphi(z|s) \parallel \tilde{p}(z)) \\ &\quad + \mathbb{E}_{z \sim \tilde{q}_\varphi(s|z)} [\log \tilde{p}_\varphi(s|z)], \end{aligned} \quad (17)$$

where $i \in \{1, \dots, M\}$ is the i^{th} sample in a dataset with a total size M , K is the set size of means μ_j and standard deviations σ_j generated by the VAE encoder, $\tilde{q}_\varphi(z|s)$ is the distribution of the VAE encoder output semantic information, $\tilde{p}(z)$ the distribution of a real image's semantic information, $\tilde{p}_\varphi(s|z)$ is the distribution of the VAE decoder output, and D_{KL} is the cross-entropy.

To achieve the efficient generation and transmission of high-quality content, the pre-training of the diffusion model in the semantic generation module is the crucial part. The corresponding objective of the information generator is to predict the noise distribution in the extracted semantic information as follows

$$loss_2 = \mathbb{E}_{\mathcal{E}(s), \epsilon \sim \mathcal{N}(0, I), t} [\|\epsilon - \epsilon_\theta(z, t|z_{text})\|_2^2]. \quad (18)$$

For the fine-tuning module, the training objective is similar to (18), except its UNet is trained to learn the distribution of the channel noise plus semantic noise.

IV. INTELLIGENT WORKLOAD TRADE-OFF SCHEME DESIGN

Considering the dynamic nature of resource availability and channel quality in wireless networks, as well as varying user preferences, it becomes essential to flexibly adapt the transmitter and receiver workload, thus catering to the service needs effectively. In this section, we introduce the performance evaluation metrics of the T2I service. Next, we present the problem formulation of the workload allocation between the edge transmitter and local receiver. Then, we propose a dueling double deep Q network (D3QN)-based scheme, namely the ROOT scheme, to make workload trade-off by adjusting the denoising steps of transmitter and receiver.

A. T2I Service Evaluation Metrics

In our SemAIGC framework, image quality and latency are the two crucial performance metrics that affect service quality. The image quality is primarily influenced by semantic similarity and reconstruction likelihood. We can fetch the image quality score by evaluating the loss between the SemAIGC image and the target image¹, as defined in (17). Meanwhile, the latency of accessing T2I service by the local receiver j from edge transmitter i consists of transmission delay $L_1^{i,j}$,

edge computing delay $L_2^{i,j}$, and local computing delay $L_3^{i,j}$, i.e., $L_{i,j} = L_1^{i,j} + L_2^{i,j} + L_3^{i,j}$. Let $O_{i,j}$ denote the data size of semantic information transmitted by edge transmitter i to local receiver j , then the transmission delay is

$$L_1^{i,j} = \frac{O_{i,j}}{v_{i,j}}, \quad (19)$$

where $v_{i,j} = B_{i,j} \cdot \log_2(1 + SNR_{i,j})$ is the bit transmission rate of the link from transmitter i to receiver j , $SNR_{i,j}$ is the signal-to-noise-ratio (SNR) of this link, and $B_{i,j}$ represents the bandwidth allocated to the link between transmitter i and receiver j .

For the computing delay, the computing speed of edge transmitter i is majorly dependent on the GPU². Let ν_i represent the processing capability (i.e., the GPU/CPU frequency in cycles/s) of each core of the GPU, and m_i denotes the GPU core number of edge transmitter i . Since almost all the computing delay is caused by the reverse diffusion process of the semantic generation module and fine-tuning module, we denote the delay resulting from other modules as a small constant l [28]. Meanwhile, the computing workload of the reverse diffusion process can be described by three factors, i.e., $\{W_i(T), O_s, \tau\}$, where $W_i(T)$ is the processing density (in GPU/CPU cycles/bits) of the transmitter UNet, O_s is the input data size, and τ ($0 \leq \tau \leq 1$) stands for the parallelizable fraction of AIGC task. Notably, $W_i(T)$ is corresponding to the total denoising step number T of the semantic generation module. According to Amdahl's law, the computing delay consists of the computing time of the serialized part and the computing time of the parallelizable part [29]. Therefore, the edge computing delay is calculated as

$$\begin{aligned} L_2^{i,j} &= \frac{(1-\tau)W_i(T)O_s}{\nu_i} + \frac{\tau W_i(T)O_s}{\nu_i m_i} + l \\ &= \frac{W_i(T)O_s}{\nu_i} \left(1 - \tau + \frac{\tau}{m_i}\right). \end{aligned} \quad (20)$$

The local computing delay $L_3^{i,j}$ is calculated in the same way. Compared with the typical edge AIGC framework, which relies on the edge transmitter to generate images and transmit them to a receiver without semantic communication, the SemAIGC framework is capable of delivering reduced service access latency when the information compression rate meets the condition in Proposition 2.

Proposition 2. *Assuming identical channel quality and resource allocation under the SemAIGC framework and the edge AIGC framework, when the compression rate of AIGC encoder is*

$$\frac{Q_{i,j}}{Q_s} < \left| 1 - \frac{W_j(\bar{T})v_{i,j}[C_1\nu_i - C_2\nu_j]}{\nu_i\nu_j + W_j(\bar{T})v_{i,j}[C_1\nu_i - C_2\nu_j]} \right|, \quad (21)$$

the SemAIGC framework provides lower service latency than the edge AIGC framework, i.e., $L^{i,j} < L_{edge}$. Here, C_1 and C_2 are constants, and $0 < C_1 < 1$, $0 < C_2 < 1$.

¹In practice, if there is no target image available, the aesthetics scores predictor can be used to evaluate the image quality in model training and image generation [27].

²The GPUs work within an ideal environment with suitable device temperature, enough graphics memory, and ample processing memory.

Proof: When the SemAIGC framework provides lower latency than the edge AIGC framework $L < L_{edge}$, we have

$$\frac{O_{i,j}}{v_{i,j}} + \frac{W_i(T)O_s}{\nu_i} \left(1 - \tau + \frac{\tau}{m_i}\right) + \frac{W_j(\bar{T})O_{i,j}}{\nu_j} \left(1 - \tau + \frac{\tau}{m_j}\right) < \frac{O_s}{v_{i,j}} + \frac{W_i(T)O_s + W_j(\bar{T})O_{i,j}}{\nu_i} \left(1 - \tau + \frac{\tau}{m_i}\right). \quad (22)$$

Then, equation (22) is transformed as follows

$$O_{i,j} \cdot \left(\frac{1}{v_{i,j}} + \frac{W_j(\bar{T})}{\nu_j} \left(1 - \tau + \frac{\tau}{m_j}\right) - \frac{W_j(\bar{T})}{\nu_i} \left(1 - \tau + \frac{\tau}{m_i}\right) \right) < O_s \cdot \frac{1}{v_{i,j}}. \quad (23)$$

Since τ , m_i and m_j are constants, given that $\frac{Q_{i,j}}{Q_s} > 0$, we prove Proposition 2. ■

B. Computing Workload Allocation Problem Formulation

Considering the dynamic resource availability, channel quality, and service requirements, we formulate the workload allocation problem as a Markov decision processing (MDP) problem. Within this context, we adjust the reverse diffusion step numbers of the semantic generation module and fine-tuning module, thus improving the utilization of the unevenly distributed computational resources and constrained communication resources to deliver suitable T2I services. The action, state, reward, and objective function of this problem is defined as follows.

Action: In this work, the edge transmitter acts as the agent to decide its encoding workload. We denote $a \in [0, \hat{T}]$ as the action, which is the reverse diffusion steps taken charge by the edge transmitter's encoder. Here, \hat{T} is the largest reverse diffusion step for image generation. Meanwhile, the total reverse diffusion step number of the local receiver is decided by a heuristic algorithm. The step of reverse diffusion in the fine-tuning module is first set to $\hat{T} - a$, if the content quality meets the requirement when $\bar{T} < \hat{T} - a$, the receiver ends the fine-tuning process early to output an image.

State: The state of system is denoted as $x = \{\bar{W}_i, \bar{W}_j, \overline{SNR}_{i,j}, \bar{\nu}_i, \bar{\nu}_j, \bar{B}_{i,j}, \bar{L}_j\}$, where \bar{W}_i and \bar{W}_j represent the average processing density of edge transmitter i and local receiver j , respectively. Moreover, $\bar{\nu}_i$ and $\bar{\nu}_j$ are the average processing capability of transmitter i and receiver j , $\overline{SNR}_{i,j}$ denotes the average SNR of the link from transmitter i to receiver j , $\bar{B}_{i,j}$ is the average bandwidth allocated by transmitter i to receiver j , and \bar{L}_j represents the average delay requirement of receiver j .

Reward and objective function: In order to provide a required image quality with target latency according to the specific requirements of the receiver, the reward function is set as

$$R = \begin{cases} 1, & L_j < \check{L}_j, \\ \frac{\check{L}_j - L_j}{\check{L}_j - \hat{L}_j}, & \check{L}_j < L_j < \hat{L}_j, \\ 0, & \text{otherwise.} \end{cases} \quad (24)$$

Here, $[\check{L}_j, \hat{L}_j]$ is the delay requirement of receiver j .

Algorithm 1 The training the processes of proposed ROOT scheme

- 1: Initialize the parameter of two networks ω and $\bar{\omega}$, the discount rate γ , the minibatch size m_D , and time $t = 0$;
- 2: **for** Episode 1 to the maximum training episode **do**
- 3: Decide an action a according to estimated Q-value under state x ;
- 4: Start the SemAIGC image generation
- 5: Execute transmitter workload according to action a ;
- 6: Transmit image semantic information;
- 7: Execute receiver workload according to the heuristic algorithm decision;
- 8: Observe reward r , and update state x' ;
- 9: Store transition (x, a, r, x') into replay buffer;
- 10: Experience replay: Sample random minibatch of transitions (x^i, a^i, r^i, x^{i+1}) from the replay buffer;
- 11: **for** $i = 1$ to m_D **do**
- 12: Computer the target value $y^i = r^i + \gamma Q_{\omega}(x^{i+1}, \text{argmax}(\mathcal{Q}(x^{i+1}, a^{i+1}; \omega^i)))$;
- 13: Update the Q-network $\omega \leftarrow \omega - a \cdot \frac{1}{m_D} \sum_{i \in m_D} [y^i - \mathcal{Q}(x^i, a^i)] \cdot \nabla_{\omega} \mathcal{Q}_{\omega}(x^i, a^i)$.
- 14: **end for**
- 15: **end for**

C. ROOT Scheme

To solve the aforementioned MDP problem, we propose the ROOT scheme, in which computing latency trade-off is achieved by dynamically adjusting the computing workload allocated to the edge transmitter and local receiver. Given the discrete action space in this scenario, a suitable approach is to employ a value-based DRL method. The D3QN has demonstrated remarkable performance to solve problems with discrete action spaces [30]. It effectively mitigates the issue of overestimation of action values in the Q-learning model and can be further enhanced by incorporating the decaying ε -greedy strategy in the policy learning. Therefore, we apply the D3QN to obtain the optimal action value estimation and efficiently choose the optimal trade-off policy.

The D3QN is an algorithm for the integration of double Q-learning and dueling DQN, its architecture is the same as dueling DQN, which is composed of two networks. One network with parameter ω is used to estimate the state value function $V(x)$ and the other with parameter $\bar{\omega}$ is used to represent the state-dependent action advantage function $\Lambda(x, a)$ [30], and then the outputs of the two separate networks can be integrated as follows:

$$\mathcal{Q}(x, a; \omega) = V(x; \omega) + \Lambda(x, a; \bar{\omega}) - \frac{1}{|A|} \sum \Lambda(x, a'; \bar{\omega}), \quad (25)$$

where a' is the next action.

For action selection, the ε -greedy strategy is utilized to balance the exploration and exploitation where the transmitter selects an action a randomly with probability ε or selects an action $a = \text{argmax}_a \mathcal{Q}(x, a; \omega) = \text{argmax}_a \Lambda(x, a; \bar{\omega})$ with probability $1 - \varepsilon$. After resource trade-off, the state, action, reward, and the next state (x, a, r, x') are stored as transitions

in replay buffer for model training. In each training iteration, there are $m_{\mathcal{D}}$ transitions used in training, and the target is computed as

$$y_i = r_i + \gamma \mathcal{Q}_{\omega}(x_{i+1}, \text{argmax}(\mathcal{Q}(x_{i+1}, a_{i+1}; \omega_i))), i \in m_{\mathcal{D}}. \quad (26)$$

The Q-network is updated according to a gradient descent step

$$\omega \leftarrow \omega - a \cdot \frac{1}{m_{\mathcal{D}}} \sum_{i=1}^{m_{\mathcal{D}}} [y_i - \mathcal{Q}(x_i, a_i)] \cdot \nabla_{\omega} \mathcal{Q}_{\omega}(x_i, a_i). \quad (27)$$

The training process of the ROOT scheme is presented in Algorithm 1.

With the D3QN, the transmitter can intelligently decide the denoising step numbers of the semantic generation module. Then, a heuristic algorithm is used to decide the total denoising steps taken by the receiver's fine-tuning module. The D3QN directly determines the action of the transmitter and implicitly affects the denoising steps decision of the receiver, because the state data contains information such as the processing capability and processing density of both the transmitter and the receiver.

V. SIMULATION RESULTS AND DISCUSSIONS

In this section, we conduct simulations to evaluate the performance of the proposed SemAIGC framework and its ROOT scheme under different scenarios. In order to demonstrate the rationality of combining SC and AIGC, we compare the proposed SemAIGC framework with the following three benchmarks.

- 1) Non-ROOT SemAIGC: This framework is identical to SemAIGC, except the ROOT scheme is disabled.
- 2) Non-fine-tuning AIGC: This framework offers a straightforward application of SemCom to the AIGC transmitter-receiver, which is similar to SemAIGC, but lacks a fine-tuning module in the receiver.
- 3) Edge AIGC: The image is generated by the T2I model deployed in BS's edge server and uses traditional bit-level transmission delivered to UE.
- 4) Local AIGC: This framework uses local UE to compute all the processes of T2I generation, in which no wireless communication is involved.

A. Simulation Settings

In the simulation, a workstation with the GPU RTX A6000 acts as the edge transmitter, and a laptop with the GPU of RTX1080 Ti acts as the local receiver. The bandwidth of BS provided for UE does not exceed 20 MHz, and the SNR is set to a range of $[-6, 15]dB$. Additionally, the latency requirement of the UE is within the range of $[5, 25]s$. The satisfaction score is issued according to the latency for the UE to fetch appropriate image quality from BS with a range of $[0, 1]$. If the generation time cost of one image exceeds the default maximum number of 60s, the task is automatically ended and determined as failed.

The model training is composed of two major parts, i.e., SemAIGC model training and ROOT scheme training. For the

SemAIGC model, the *Stable Diffusion v1-5* model checkpoint is used in the pre-trained model [18]. The corresponding semantic extraction module of text is encoded by pre-trained OpenAI CLIP [20]. Meanwhile, the pre-trained VAE encoder and decoder are used as the image semantic extraction module and autoencoder decoder module, respectively [26]. In this work, to adjust the UNet weights of the fine-tuning module, a subset within the *laion-aesthetics v2 5+* is used, which contains high-resolution figures, and corresponding caption texts. In training, all the images of this subset are filtered to a size of $512 \times 512 \times 3$. Meanwhile, the evaluation is conducted by using a validation set with 500 images. All the pre-processed images are extracted as $1 \times 4 \times 64 \times 64$ image semantic information by VAE encoder for UNet training. Moreover, the UNet is trained with 1 middle block in 8×8 resolution, 12 encoding blocks, and 12 decoding blocks in 4 resolutions, i.e., 64×64 , 32×32 , 16×16 , and 8×8 [18].

For the D3QN setting in the ROOT scheme, both the DQN network and target network have an input layer with 7 neurons and a 10-neural output layer, as well as 2 hidden layers with each of 256 neurons [30]. We employ *ReLU* as the activation function between the input layer and the two hidden layers. The training minibatch size is set to 64, and the reward discount rate is set to 0.99.

We first examine the generated image quality of different AIGC generation and transmission frameworks under different channel qualities, shown in Fig. 4 and Fig. 5. Notably, since the number of denoising steps can affect image quality, for fairness, we ought to set the denoising step of different frameworks into the same number. However, the SemAIGC tends to intelligently adjust the denoising step of the transmitter and receiver. Hence, here we use DRL-disabled Non-ROOT SemAIGC to compare with edge AIGC and non-fine-tuning AIGC. The result of local AIGC is not shown since it is not impacted by channel quality. In the Non-ROOT SemAIGC service, both the denoising step of the semantic generation module and that of the fine-tuning module are set to 15, while the total denoising step of the other two frameworks is 30 for each. As shown in Fig. 4, it is obvious that the images generated by Non-ROOT SemAIGC exhibit excellent clarity, and accurate colors, and align seamlessly with the textual description. The Non-ROOT SemAIGC outperforms the Non-fine-tuning AIGC system under all channel quality while generating images with structures that nearly resemble those of the edge AIGC, thanks to the fine-tuning model's effective channel noise reduction and preservation of valuable semantic information. Moreover, we compared the image details of Non-ROOT SemAIGC and the other two frameworks under a 0 dB channel in Fig. 5. It is observed that the SemAIGC can output the clearest image with a smooth texture, while other frameworks' images have noisy points and blurred edges. The results further indicate that the proposed SemAIGC is effective and robust in generating high-quality images.

In this work, we aim to provide suitable image quality with adaptable latency for UE while taking communication resources, computational resources, and channel quality into consideration. Before delving into an analysis of SemAIGC's latency performance, we scrutinize its convergence perfor-

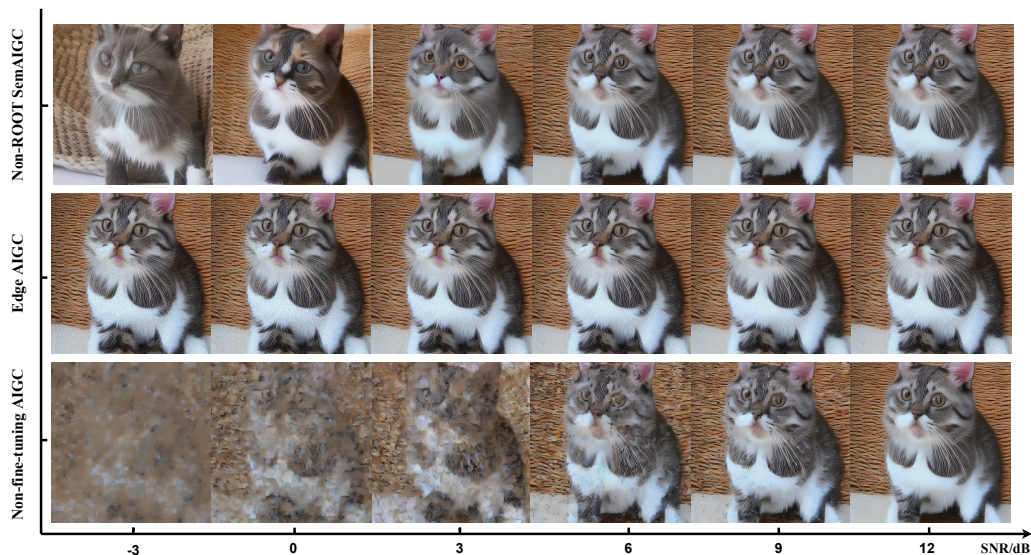


Fig. 4. The delivered images of three AIGC generation and transmission frameworks under different SNR (text input: “A cute furry cat”).

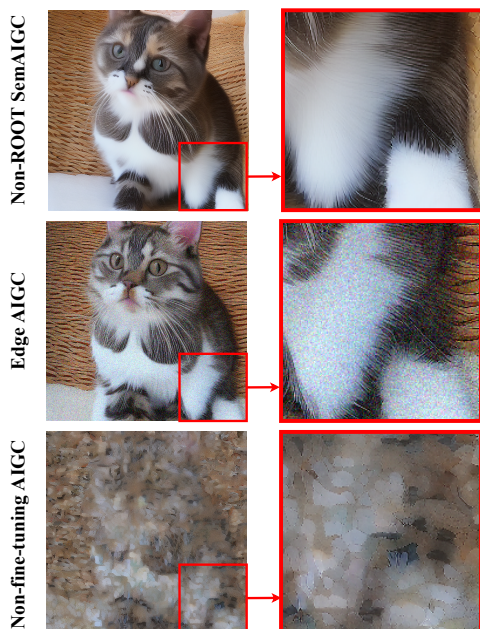


Fig. 5. The image details of three AIGC generation and transmission frameworks under 0dB wireless channel.

mance by comparing its average reward with that of four alternative benchmarks, as shown in Fig. 6. It is worth noting that these four benchmarks employ the same reward function as the SemAIGC framework. We observe that SemAIGC excels in terms of convergence speed, achieving convergence in approximately 350 episodes. This superior performance can be attributed to the ROOT scheme within the SemAIGC framework, which intelligently allocates workload for BS and UE based on available resources and channel quality.

Fig. 7 illustrates the average satisfaction score of UE when using the SemAIGC framework, in response to dynamic changes in channel quality and the percentages of available

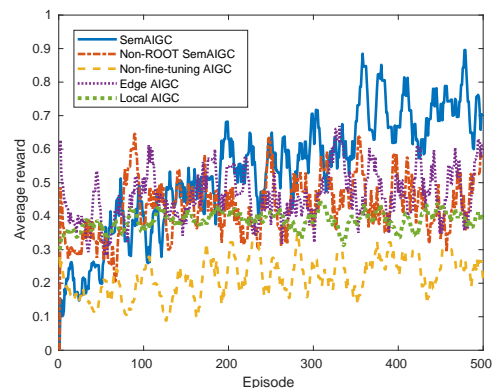


Fig. 6. Convergence performance for four AIGC generation and transmission framework.

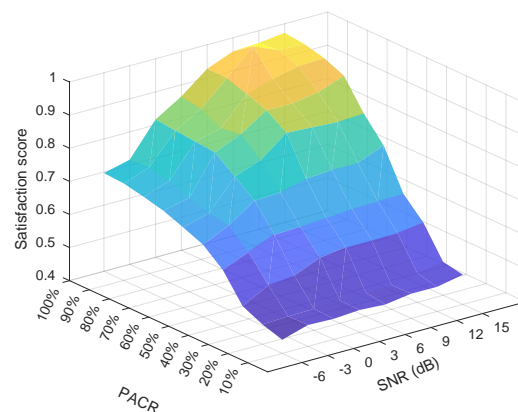
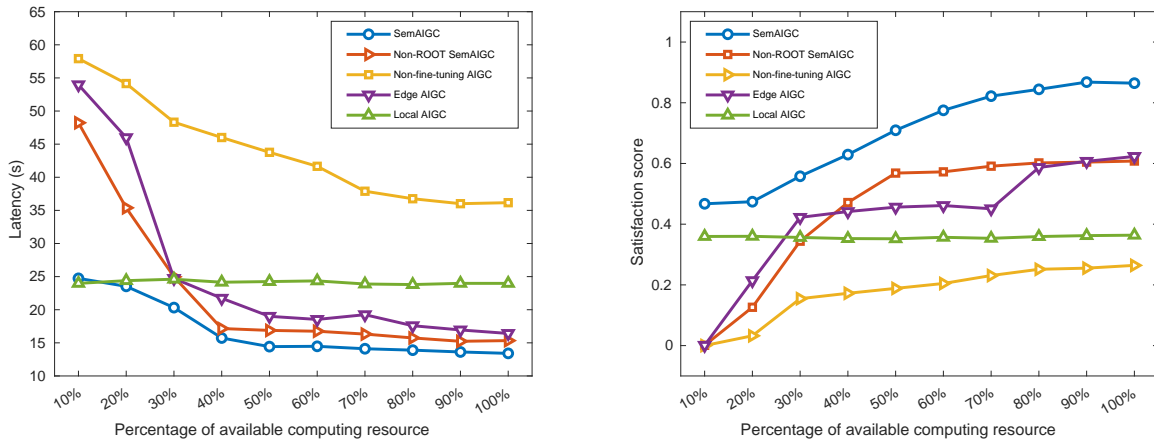
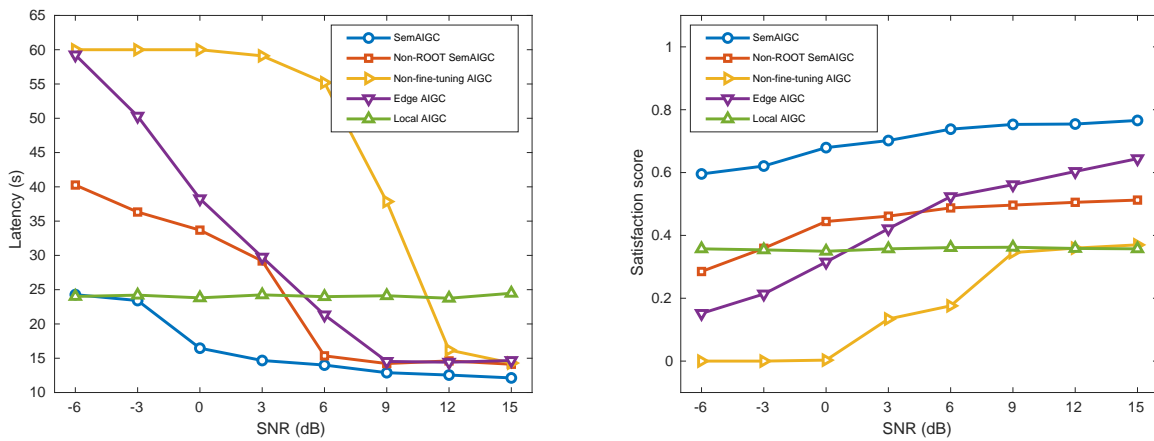


Fig. 7. Satisfaction score for the SemAIGC framework under dynamic computing power and channel qualities.



(a) Average latency under different percentages of computing power. (b) Satisfaction score under different percentages of computing power.



(c) Average latency under different SNRs.

(d) Satisfaction score under different SNRs.

Fig. 8. Service quality experienced by UEs for four different frameworks.

computing resources (PACR) for BS. Notably, the satisfaction score exhibits an increase, ranging from approximately 45% to 98%, in tandem with the percentage of available computing resources for BS and Signal-to-Noise Ratio (SNR). Although under the most challenging conditions, characterized by the poorest channel quality with an SNR of -6 dB, SemAIGC can still attain an acceptable satisfaction score of approximately 70%, provided that BS possesses sufficient computational resources. This impressive performance can be attributed to that the BS with ample computing power can speedily generate semantic information, and the fine-tuning module can effectively and promptly mitigate channel noise while preserving valuable semantic information.

To further demonstrate the performance of SemAIGC, we conduct a comparative analysis of its average latency and satisfaction score with four other AIGC generation and transmission frameworks, as depicted in Fig. 8.

As seen in Fig. 8(a), when computational resources are fixed and the Signal-to-Noise Ratio (SNR) varies dynamically, SimAIGC consistently maintains an average latency below 25 s, surpassing the performance of the other three frameworks. This superiority is even more pronounced in Fig.

8(b). Although SemAIGC exhibits a slightly lower average latency than Edge AIGC by a mere 2 s, its satisfaction rate outperforms Edge AIGC by approximately 40%. This is due to the fact that SemAIGC prioritizes delivering images within a required time range rather than blindly pursuing extremely low latency. Furthermore, Fig. 8(c) and Fig.8(d) offer insights into the performance of these frameworks under varying SNR conditions. In Fig. 8(c), it becomes evident that in scenarios with poor channel quality, the UE of both the non-fine-tuning AIGC and Edge AIGC framework experience significantly higher latency, approximately 25 s and 45 s greater than that of SemAIGC, respectively. This disparity arises from the absence of UNet, which is responsible for denoising received information from the UE side and ensuring suitable image quality within the given time constraints. Additionally, from Fig. 8(d), it is more obvious that the other four frameworks cannot provide a satisfying service as the SemAIGC, which further validates the effectiveness of introducing DRL.

VI. CONCLUSION

In this paper, we introduce the SemAIGC framework as a novel approach for jointly generating and transmitting content

in wireless networks where communication resources are limited and computational resources are distributed unevenly. Our framework employs SemCom to reduce the consumption of communication resources. In addition, diffusion models are deployed into the encoder and decoder to develop a workload-adjustable transceiver and improve the utilization of computational resources. Furthermore, a ROOT scheme is presented in SemaAIGC to intelligently make workload trade-off decisions for providing adaptive AIGC access service. Simulations are conducted under dynamic resource availability, channel quality, and service requirement, where numerical results demonstrate the service quality and robustness improvement of our proposed SemaAIGC framework.

This paper promises to be a seminal work providing valuable inspiration for future research in the realm of wireless AIGC provisioning. For instance, the utilization of SemCom may prove instrumental in efficiently managing communication and computational resources in resource-intensive AIGC networks. Moreover, the generative AI model employed in this work can inspire the development of novel methods for semantic extraction, transmission, and recovery in the domain of image SemCom.

REFERENCES

- [1] A. Jo, "The promise and peril of generative ai," *Nature*, vol. 614, no. 1, pp. 214–216, 2023.
- [2] Y. Wang, Y. Pan, M. Yan, Z. Su, and T. H. Luan, "A survey on chatgpt: Ai-generated contents, challenges, and solutions," *arXiv preprint arXiv:2305.18339*, 2023.
- [3] L. Xia, Y. Sun, C. Liang, L. Zhang, M. A. Imran, and D. Niyato, "Generative AI for Semantic Communication: Architecture, Challenges, and Outlook," *arXiv preprint arXiv:2308.15483*, 2023.
- [4] F. J. G. Peñalvo, A. Sharma, A. Chhabra, S. K. Singh, S. Kumar, V. Arya, and A. Gaurav, "Mobile cloud computing and sustainable development: Opportunities, challenges, and future directions," *International Journal of Cloud Applications and Computing (IJCAC)*, vol. 12, no. 1, pp. 1–20, 2022.
- [5] M. Xu, H. Du, D. Niyato, J. Kang, Z. Xiong, S. Mao, Z. Han, A. Jamalipour, D. I. Kim, V. Leung *et al.*, "Unleashing the power of edge-cloud generative ai in mobile networks: A survey of aigc services," *arXiv preprint arXiv:2303.16129*, 2023.
- [6] H. Du, Z. Li, D. Niyato, J. Kang, Z. Xiong, D. I. Kim *et al.*, "Enabling ai-generated content (aigc) services in wireless edge networks," *arXiv preprint arXiv:2301.03220*, 2023.
- [7] J. Wang, H. Du, D. Niyato, J. Kang, Z. Xiong, D. Rajan, S. Mao *et al.*, "A Unified Framework for Guiding Generative AI with Wireless Perception in Resource Constrained Mobile Edge Networks," *arXiv preprint arXiv:2309.01426*, 2023.
- [8] H. Park, A. Yessenbayev, T. Singhal, N. K. Adhikari, Y. Zhang, S. M. Borse, H. Cai, N. P. Pandey, F. Yin, F. Mayer *et al.*, "Real-time, accurate, and consistent video semantic segmentation via unsupervised adaptation and cross-unit deployment on mobile device," in *Proceedings of the IEEE/CVF Conference on Computer Vision and Pattern Recognition*, 2022, pp. 21 431–21 438.
- [9] Z. Sun, H. Yu, X. Song, R. Liu, Y. Yang, and D. Zhou, "Mobilebert: a compact task-agnostic bert for resource-limited devices," *arXiv preprint arXiv:2004.02984*, 2020.
- [10] H. Du, R. Zhang, D. Niyato, J. Kang, Z. Xiong, D. I. Kim, H. V. Poor *et al.*, "Exploring collaborative distributed diffusion-based ai-generated content (aigc) in wireless networks," *arXiv preprint arXiv:2304.03446*, 2023.
- [11] Z. Qin, X. Tao, J. Lu, and G. Y. Li, "Semantic communications: Principles and challenges," *arXiv preprint arXiv:2201.01389*, 2021.
- [12] D. Huang, X. Tao, F. Gao, and J. Lu, "Deep learning-based image semantic coding for semantic communications," in *2021 IEEE Global Communications Conference (GLOBECOM)*. IEEE, 2021, pp. 1–6.
- [13] B. Güler, A. Yener, and A. Swami, "The semantic communication game," *IEEE Transactions on Cognitive Communications and Networking*, vol. 4, no. 4, pp. 787–802, 2018.
- [14] D. B. Kurka and D. Gündüz, "Bandwidth-agile image transmission with deep joint source-channel coding," *IEEE Transactions on Wireless Communications*, vol. 20, no. 12, pp. 8081–8095, 2021.
- [15] S. Wang, J. Dai, Z. Liang, K. Niu, Z. Si, C. Dong, X. Qin, and P. Zhang, "Wireless deep video semantic transmission," *IEEE Journal on Selected Areas in Communications*, vol. 41, no. 1, pp. 214–229, 2022.
- [16] Z. Lin, Y. Gong, Y. Shen, T. Wu, Z. Fan, C. Lin, N. Duan, and W. Chen, "Text Generation with Diffusion Language Models: A Pre-Training Approach with Continuous Paragraph Denoise," in *International Conference on Machine Learning*. PMLR, 2023, pp. 21 051–21 064.
- [17] R. Huang, Z. Zhao, H. Liu, J. Liu, C. Cui, and Y. Ren, "Prodiff: Progressive Fast Diffusion Model for High-Quality Text-to-Speech," in *Proceedings of the 30th ACM International Conference on Multimedia*, 2022, pp. 2595–2605.
- [18] R. Rombach, A. Blattmann, D. Lorenz, P. Esser, and B. Ommer, "High-resolution image synthesis with latent diffusion models," in *Proceedings of the IEEE/CVF conference on computer vision and pattern recognition*, 2022, pp. 10 684–10 695.
- [19] H. Hu, D. Wu, F. Zhou, X. Zhu, R. Q. Hu, and H. Zhu, "Intelligent resource allocation for edge-cloud collaborative networks: A hybrid ddpq-d3qn approach," *IEEE Transactions on Vehicular Technology*, 2023.
- [20] A. Radford, J. W. Kim, C. Hallacy, A. Ramesh, G. Goh, S. Agarwal, G. Sastry, A. Askell, P. Mishkin, J. Clark *et al.*, "Learning transferable visual models from natural language supervision," in *International conference on machine learning*. PMLR, 2021, pp. 8748–8763.
- [21] D. P. Kingma and M. Welling, "Auto-encoding variational bayes," *arXiv preprint arXiv:1312.6114*, 2013.
- [22] J. Ho, A. Jain, and P. Abbeel, "Denosing Diffusion Probabilistic Models," *Advances in neural information processing systems*, vol. 33, pp. 6840–6851, 2020.
- [23] O. Ronneberger, P. Fischer, and T. Brox, "U-net: Convolutional networks for biomedical image segmentation," in *Medical Image Computing and Computer-Assisted Intervention—MICCAI 2015: 18th International Conference, Munich, Germany, October 5-9, 2015, Proceedings, Part III 18*. Springer, 2015, pp. 234–241.
- [24] P. Jiang, C.-K. Wen, S. Jin, and G. Y. Li, "Deep source-channel coding for sentence semantic transmission with harq," *IEEE transactions on communications*, vol. 70, no. 8, pp. 5225–5240, 2022.
- [25] Y. Li, H. Wang, Q. Jin, J. Hu, P. Chemerys, Y. Fu, Y. Wang, S. Tulyakov, and J. Ren, "Snapfusion: Text-to-image diffusion model on mobile devices within two seconds," *arXiv preprint arXiv:2306.00980*, 2023.
- [26] D. P. Kingma, T. Salimans, R. Jozefowicz, X. Chen, I. Sutskever, and M. Welling, "Improved variational inference with inverse autoregressive flow," *Advances in neural information processing systems*, vol. 29, 2016.
- [27] V. Hosu, B. Goldlucke, and D. Saupé, "Effective aesthetics prediction with multi-level spatially pooled features," in *proceedings of the IEEE/CVF conference on computer vision and pattern recognition*, 2019, pp. 9375–9383.
- [28] A. Sauer, T. Karras, S. Laine, A. Geiger, and T. Aila, "Stylegan-t: Unlocking the power of gans for fast large-scale text-to-image synthesis," *arXiv preprint arXiv:2301.09515*, 2023.
- [29] Q. Luo, S. Hu, C. Li, G. Li, and W. Shi, "Resource Scheduling in Edge Computing: A Survey," *IEEE Communications Surveys & Tutorials*, vol. 23, no. 4, pp. 2131–2165, 2021.
- [30] Z. Wang, T. Schaul, M. Hessel, H. Hasselt, M. Lanctot, and N. Freitas, "Dueling network architectures for deep reinforcement learning," in *International conference on machine learning*. PMLR, 2016, pp. 1995–2003.